Eco-friendly laccase and cellulase enzymes pretreatment for optimized production of high content lignin-cellulose nanofibrils

Matheus Cordazzo Dias, Mohamed Naceur Belgacem, Jaime Vilela de Resende, Maria Alice Martins, Renato Augusto Pereira Damásio, Gustavo Henrique Denzin Tonoli, Saulo Rocha Ferreira

ECO-FRIENDLY LACCASE AND CELLULASE ENZYMES PRETREATMENT FOR OPTIMIZED PRODUCTION OF HIGH CONTENT LIGNIN-CELLULOSE NANOFIBRILS

Matheus Cordazzo Dias[1,2], Mohamed Naceur Belgacem[2], Jaime Vilela de Resende[3], Maria Alice Martins[4], Renato Augusto Pereira Damásio[5], Gustavo Henrique Denzin Tonoli[1], Saulo Rocha Ferreira[6*]

1 Department of Forest Science, Federal University of Lavras, C.P. 3037, 37200-900, Lavras, MG, Brazil

2 Université Grenoble Alpes, CNRS, Grenoble INP (Institute of Engineering Univ. Grenoble Alpes), LGP2, 38000, Grenoble, France

3 Department of Food Science, Federal University of Lavras, C.P. 3037, 37200-900 Lavras, MG, Brazil

4 Nanotechnology National Laboratory for Agriculture, Embrapa Instrumentation, 13560-970, São Carlos, SP, Brazil

5 Klabin, Technology Center, Industrial R&D+I, Fazenda Monte Alegre, St. Harmonia, 84275-000 - Telêmaco Borba, PR, Brazil

6 Department of Engineering, Federal University of Lavras, C.P. 3037, 37200-900 Lavras, MG, Brazil

***Corresponding author:** Matheus Cordazzo Dias, Department of Forest Science, Federal University of Lavras, C.P. 3037, 37200-900, Lavras, MG, Brazil, e-mail: matheus.cordasso@gmail.com

Graphical abstract:

Graphical abstract here, please

Abstract: Lignin-cellulose nanofibrils (LCNF) are of attracting an increasing interest due to the benefits of maintaining the lignin in the nanomaterial composition. The production of LCNF requires considerable energy consumption, which has been suppressed employing pretreatment of biomass, in which it highlights those that employ enzymes that have the advantage of being more environmentally friendly. Some negative aspects of the presence of lignin in the fiber to obtain cellulose nanofibrils is that it can hinder the delamination of the cell wall and act as a physical barrier to the action of cellulase enzymes. This study aimed to evaluate the impact of a combined enzymatic pretreatment of laccase and endoglucanase for high content lignin LCNF production. The morphological and chemical properties, visual aspect and stability, crystallinity, mechanical properties, rheology, barrier properties and quality index were used to characterize the LCNF. The laccase loading used was efficient in modifying the lignin to facilitate the action of the endoglucanase on cellulose without causing the removal of this macromolecule. This pretreatment improved the quality of LCNF (61 ± 3 to 71 ± 2 points) with an energy saving of 42% and, therefore, this pretreatment could be suitable for industrial production for a variety of applications.

Keywords: Cell wall. Cellulose nanofibers. Enzymatic hydrolysis. Lignin. Nanofibrillated cellulose.

1. Introduction

Cellulose nanofibrils (CNF) have been widely studied for the most diverse applications as substitutes for synthetic and non-biodegradable polymers, and almost always, the raw source to produce of this material has been bleached cellulosic pulps, as it is reported that lignin is considered an obstacle in the nanofibrillation process [1]. Lignin is linked to hemicellulose through covalent bonds, at the carbon-α and C-4 positions on the benzene ring. Presumably, small-scale intermolecular chemical bonds of lignin-carbohydrates exist natively between lignin, hemicellulose, and cellulose [2]. Its monomers' properties and the inter polymer interactions cause this structure to present biological, chemical, and mechanical resistance, hindering separation and recovery of its three main components, characterizing recalcitrance [3].

Compared to the production of CNF from bleached pulp, LCNF presents as an advantage the resource and energy savings from the suppression of the pulp bleaching step, making it a promising material to be used on an industrial scale [4,5]. The presence of lignin in the nanofibrils matrix improves the hydrophobicity and thermal stability of cellulose nanofibrils, benefitting the compatibility with various hydrophobic polymers [6]. It's presence also have shown advantages in composite reinforcement and pickering emulsions [7]. Furthermore, because lignin has an excellent natural ability to block UV radiation, the potential use of LCNF instead of CNF is advantageous in clean windows, anti-counterfeiting materials, and windshields for vehicles [8].

Thus, for the most effective use of this plant biomass, it is essential to carry out pretreatments to make cellulose more accessible by modifying its physical and chemical structure, facilitating the conversion of vegetal fibers into several bio-products [9]. Many chemical and enzymatic pretreatments have been widely researched and applied for the most economical production of nanocellulose. More recently, enzymatic pretreatments have attracted more interest due to the increasing interest in the impacts that chemical reagents may cause in the environment and the expenses for their recovery and recycling. On the other hand, enzymes present high specificity, low enzymatic load for action and mild reaction condition, besides not producing dangerous chemical residues [5].

The first studies on enzymatic pretreatments to facilitate the obtainment of cellulose nanofibrils were developed by Henriksson et al. and Pääkko et al. [10,11], since then, many studies have been developed using cellulase enzymes [12–14], and other enzyme classes, such as xylanases [5,15], lytic polysaccharide monooxygenase (LPMO) [16], and the mixture of these enzymes. Endoglucanase and xylanase were applied together by Bian et al. [5] to obtain LCNF. Besides removing the surface xylan from the fiber, the study demonstrated that this pretreatment provided LCNF with smoother surface, higher tensile strength, and Young's modulus.

Cellulose enzymatic hydrolysis requires physical contact between glycosidic hydrolases and their substrates, which can be obstructed by lignin in several ways [17]. In unbleached pulps, insoluble lignin can block enzyme access to carbohydrate surfaces, its structure can inhibit the action of enzymes in cellulose through physical barriers, such as hydrophobicity, surface charges, electrostatic interactions, and interactions between hydrogen bonds, limiting the accessibility of enzymes, decreasing enzyme yield [18]. The fate of the catalytic activity of the adsorbed cellulases is under debate since there are reports of cellulases linked to lignin retaining most of their activity [19].

Laccase enzymes have emerged as important biotechnological catalysts for their ecological nature and mild working conditions. They are multi-copper enzymes capable of catalyzing the direct oxidation of a wide range of aromatic compounds, such as lignin monomers, of generating reactive radicals, and using molecular oxygen as an oxidizer [20]. However, Steinmetz et al.[21] demonstrated the potential of laccase as a depolymerizing agent of lignin in a semi-continuous process in mild conditions. Laccases have been researched in the paper industry as a bleaching agent [22], as a lignin modifier to improve the mechanical properties of kraft papers [23] and as a pretreatment to obtain cellulose nanofibril in an oxidative system along with TEMPO [24].

In this context, this study aims to evaluate the effectiveness of two sequential enzyme pre-steps in the cellulose nanofibrillation quality and energy consumption: 1) laccase enzyme to depolymerize lignin; and 2) cellulase enzymes to facilitate mechanical shearing actions and

investigate if it may be a viable alternative to increase the yield and quality of lignin-cellulose nanofibrils.

2. Experimental

2.1 Materials

Unbleached Eucalyptus kraft liner pulp donated by Klabin S.A. (Paraná/Brazil) was used. All the materials were used as received from the producers: acetic acid (CH_3COOH) (ACS reagent, ≥99.7%, Sigma-Aldrich, France); deionized water; endoglucanase FiberCare 4890 ECU/g enzyme solution (Novozymes, Denmark); laccase Novozym ≥1000 LAMU/g enzyme solution (Sigma-Aldrich, France); sodium acetate trihydrate ($CH_3COONa \cdot 3H_2O$) (ReagentPlus, ≥99.0%, Sigma-Aldrich, France); glycerol ($C_3H_8O_3$), (ACS reagent, ≥99.5%, Êxodo, Brazil); diiodomethane (CH_2I_2) (ReagentPlus, ≥99.0%, Sigma-Aldrich, Brazil); 1-bromonaphtalene ($C_{10}H_7Br$) (ACS reagent, ≥ 97%, Sigma-Aldrich, Brazil). ANOVA and Tukey's test at 95% significance, were applied to investigate if the averages were statistically different from the Untreated sample. Statistical analyzes were performed using the free software SISVAR version 5.6.

2.2 Characterization of the pulp fibers

Acid-insoluble lignin was determined following the standard TAPPI T222-15 and acid-soluble lignin content was evaluated following the standard TAPPI UM 250-76. Carbohydrates were determined according to the standard TAPPI T249-09. An Dionex ICS 5000 ion chromatography system (ThermoFisher, USA) was used.

The morphological properties of the fiber's suspensions were measured using a MorFi fiber and shive analyzer (TECHPAP, France). Fine elements were considered as any detected object present in the pulp with dimensions lower than 80 µm. The samples of fibers suspensions were diluted in deionized water to about 0.400 g/L, and 1 L of this suspension was poured into the MorFi and measured for five minutes. Three repetitions were performed, and the obtained results averaged.

2.3 Enzymatic pretreatments

Laccase mediated enzymatic pretreatment using a laccase commercial enzyme Novozym 51003 was performed with a concentration of 60 LAMU/g of cellulose. Refined pulp with a Schopper-Riegler degree of 70-80° were introduced at 2 wt% in a reactor pre-heated at 40°C under continuous mechanical agitation with a 300-rpm rotation speed. A pH of 4.5 was adjusted by adding an acetate buffer composed of acetic acid and sodium trihydrate. Once the temperature (40°C) and pH stabilized, an enzyme solution was poured into the reactor and left for a reaction time of 2 h. To stop the enzymatic activity, the reactor was heated to 80°C for 10 min, then cooled to 25°C. Finally, the suspension was recovered, filtered using a 1 µm nylon sieve, and rinsed with deionized water. Afterwards, previously laccase pretreated pulp was pretreated using an endoglucanase commercial enzyme FiberCare (300 ECU/g of cellulose). The pulp was introduced at 2 wt% in a reactor (50°C) under continuous mechanical agitation (300-rpm) and a pH of 5. Once the temperature and pH stabilized, the enzyme solution was poured into the reactor and left for a reaction time of 2 h. Finally, the same procedure as the previous pre-treatment was used to recover the material.

All pretreatments were coded to be easily assessed throughout the work (Table 1).

Table 1. Experimental design and coding of samples.

Fiber	Condition	Pretreatment	Code
Unbleached Eucalyptus Kraft Pulp	Before nanofibrillation	Not pretreated	UEKP
		Laccase treated	LT_UEKP
		Laccase-cellulase treated	LCT_UEKP
	After nanofibrillation	Not pretreated	ULCNF
		-	-
		Laccase-cellulase treated	EsT_LCNF

2.4 LCNF production by mechanical nanofibrillation

Refined cellulose pulps were immersed for three days in deionized water at 2 wt% to guarantee fiber swelling. Then, they were nanofibrillated by passing the pulp through an MKCA6-

2 ultra-fine grinder Supermasscolloider (disk model MKGA6-80, Masuko Sangyo, Japan). The disks speed was fixed at 1,500 rpm [25]. The gap between the grinding stones was set to 10 µm for the first three passes and then to -20 µm for the remaining passes. A three-phase wattmeter was introduced on the Masuko device to measure the total active power.

The energy used during nanofibrillation was determined with a three-phase wattmeter, which can measure total input energy using the Eq. (1):

$$TEC_{(kWh/kg)} = \frac{TIE\ (kWh)}{m\ (kg)} \quad (1)$$

TEC is the total energy consumption (kWh/kg), TIE is the total energy input, and m is the mass of cellulose pulp (kg).

2.5 Turbidity, visual inspection, stability, and Zeta potential of LCNF suspensions

The turbidity (NTU) of the LCNF suspensions was measured using a turbidimeter AL-250 (Aqualytic, Germany) on an 0.1 wt% LCNF suspension. The unity NTU refers to Nephelometric Turbidity Units.

The suspensions were diluted to 0.1 wt% and was placed in test recipients for photos acquisition. Images were acquired at 0, 10, 30 min, 1, 2, 3, 4, 5, 6, 7, 8, and 24 h. Fiji software was used to estimate LCNF decantation in the suspensions, and then stability was calculated according to Eq. 2 proposed by Silva et al. [26]:

$$Stability = \left(\frac{Dispersed}{Total}\right) \times 100\% \quad (2)$$

Where Dispersed is the height of the suspended particles, and Total is the height of the entire liquid in the recipient.

The zeta potential test was conducted with a Dynamic Zetasizer Nano ZS 90 (Malvern Panalytical Instruments, UK) at 25°C to evaluate the stabilization of LCNF suspensions (0.1 wt%).

2.6 Morphological characterization of LCNF

The LCNF suspensions were observed using a light microscope (Zeiss Axio AX10, Germany). The suspensions were previously diluted to 0.1 wt% and stirred for 1 min with Ultra Turrax T-25 (IKA, Sweden) at 10,000 rpm. Pictures were obtained using a 10x objective lens and

analyzed using Fiji software. The average size of the observable particles was extracted using the Analyze Particles function. Ten images by sample were used in this step. Transmission Electron Microscopy of the LCNF was investigated using a Tecnai G2-12 (FEI company, USA) instrument with an accelerated voltage of 80 kV. A drop of dilute LCNF suspensions (0.001%) were deposited onto a carbon-coated electron microscopy copper grid. The excess liquid suspension was removed by using filter paper, and a drop of 2% uranyl acetate was added for contrast. The grids were left to dry at room temperature. Images were post-processed using Fiji.

2.7 Nano-structured papers preparation

LCNF nano-structured papers, also called "nanopapers" were prepared with a sheet former (Xell Rapid Kothen, ISO 5269-2, PTE, Austria) from 2 g of LCNF (dry content) diluted to 0.5% in deionized water. First, the suspension was filtered in a 1 µm nylon sieve under vacuum at −600 mbar during a specific time until removing of water supernatant. Then, the sheet was dried at 85°C under 0.8 bar pressure between two 1 µm nylon sieves (one on each side) to prevent adherence and two cardboards (one on each side) for 20 min. All the nanopapers were stored for 48 h in a conditioned room at 23 ± 2°C and 50 ± 2% RH before characterization. The porosity of the nanopapers was calculated from the basis weight of each sample (kg/m2) and its thickness (µm), using the following Eq. (3) described by Desmaisons et al. [13]. The samples were cut at (50×50) mm^2 dimensions.

$$P(\%)=1-\left(\frac{BW}{e \times \rho c}\right) \times 100 \quad (3)$$

where BW is the basis weight (kg/m^2), e is the thickness (m), and ρc is the density of cellulose (1540 kg/m^3). Five replicates were performed.

2.8 X-Ray diffraction (XRD)

The XRD analyses were performed using a PANalytical X'Pert PRO MPD X-ray diffractometer (Malvern Panalytical, UK), equipped with an X'celerator detector with a Cu-Kα source (λ = 1.5406 Å) in the 2θ range of 10 - 40°. A step rate of 0.066° was used. The equipment was operated at a tension of 45 kV and a current of 40 mA.

The theoretical coordinates of native cellulose Iβ (FWHM = 0.1) were extracted from crystallography information data (.cif) using the software Mercury 2020.2.0 (CCDC, UK) obtained from the Supplementary Information accompanying the original work from Nishiyama et al. [27].

The patterns were deconvoluted using the Gaussian function with Magic Plot 2.9 (Magicplot Systems, Russia). For the amorphous halo, cellulose II pattern with peak width at half maximum (FWHM = 9), only varying its intensity, was used as suggested in the literature [28]. After deconvolution, the crystalline fraction (CF) was calculated from the ratio among the area of all the crystalline peaks and the total area of the whole curve, determined after deconvolution following Eq. (4):

$$CF(\%)=\frac{\sum Area_{Crystalline\ Peaks}}{\sum Area_{Crystalline\ Peaks}+ Area_{Amorphous\ Halo}} \quad (4)$$

The crystallite size of the (200) plane peak was calculated according to Scherrer's equation (Eq. 5):

$$D=\frac{K \times \lambda}{\beta \times \cos\theta} \quad (5)$$

Where D is crystallite size (Å), K (0.9) is a constant that refers to crystal shape, λ is the wavelength of the ray used (Copper), β is the FWHM of the peak, in radians, and θ is the Bragg's angle of (200) plane diffraction.

2.9 Mechanical properties

The tensile properties were measured with a universal testing machine (Instron 3365, USA) equipped with a load cell of 5 kN capacity, following the NF Q03-004 standard. The weight basis of the nanopaper specimens was measured using an analytical balance, and the thickness of the specimens was measured using a Lhomargy micrometer. These values were then reported into the tensile device to obtain the Young's Modulus. Tensile tests were performed at 5 mm/min, and an initial distance of 100 mm between the clamping jaws. The dimensions of the samples were 150 mm for the length and 15 mm for the width. For each sample, the minimal number of repetitions was seven and the average value was used for further calculations. The tear resistance

was measured using a tear tester (Noviprofibre, Elmendorf pendulum 4000mN, France). Samples were cut at (65×50) mm^2 dimensions, and the measurement corresponds to the force (mN) needed for tear propagation after a primer.

2.10 Rheological parameters

This step was performed according to previous work from Souza et al. [29]. The study of the rheological behavior of LCNF suspensions at 1% wt concentration was performed on a Physica MCR 301 (Anton Paar, Austria) rheometer coupled to an AWC100 (Julabo, Germany) thermostatic bath using the PP25 DIN Ti parallel plate sensor (D = 25 mm; Gap = 1 mm). The samples were submitted to flow curves using three continuous ramps (ascending, decreasing, and ascending) with a deformation rate ranging from 0 to 300 s^{-1} for 2 min for each curve at 25°C. The Herschel-Bulkley (Eq. 6) model was adjusted to the data of the second increasing curve to determine the fluid flow profile and obtain the viscosity. The model was adjusted by the software Origin 2022 (OriginLab, USA), using three repetitions.

$$\tau = \tau_0 + K \times \dot{\gamma}^{\eta} \quad (6)$$

Where τ is the shear stress in (Pa), $\tau 0$ is the yield stress in (Pa), K is the consistency index (Pa s^n), $\dot{\gamma}$ is the deformation rate (s^{-1}), and n is the flow behavior index (dimensionless).

The apparent viscosity values were evaluated at a shear rate of 100 s^{-1}, which, according to Steffe [30], corresponds to a deformation commonly suffered by fluids in industrial pipes concerning processes as pumping and agitation.

Oscillatory tests were performed according to Dimic-Misic et al.[31] to measure storage modulus (G´) and loss modulus (G´´), by angular frequency (ω) from 0.1 to 100 s^{-1}. The linear viscoelastic range (LVE) was acquired from an amplitude sweep using constant angular frequency (ω) of 1 s^{-1}, varying strain amplitude between 0.01 and 100%. Interval thixotropy test recovery measurements (3ITT) was determined according to the work of Rantanen et al.[32]. The samples were subjected to low shear rate (0.1 s^{-1}), then subsequently high shear rate (1000 s^{-1}), and finally once again low shear rate.

2.11 Contact angle, surface wettability,surface free energy and barrier properties of nanopapers

The contact angle and surface wettability of the nanopapers was determined following the standard TAPPI T458-14. This analysis was conducted using a Drop Shape Analyzer model DSA25B (Krüss, Germany) and the software ADVANCE version 1.4.1.2. The dispersive and polar components of the surface free energy of the LCNF nanopapers samples were determined according to Owens and Wendt [33] using deionized water, glycerol, and ethylene glycol as polar solvents, and diiodo-methane and 1-bromonaphtalene as apolar solvents.The water vapor transmission rate (WVTR) and water vapor permeability (WVP) were determined following the standard TAPPI T464 om-18. The nanopapers were sealed on glass containers which were placed in a controlled chamber at 37.8°C and a 90% humidity and weighted at separate times intervals to calculate the mass gain. The grease resistance of the nanopapers was determined according the standard TAPPI T559 cm-12.

2.12 Simplified quality index (Q.I*)

A quality index adapted from the previous work from Desmaisons et al. [13] was used for the comparison of LCNF suspensions together. Although the quality index (Q.I*) was developed for the analysis of enzymatic bleached CNF and not for lignin-containing CNF, it was used to obtain a broad view of the quality of the produced material. This value regroups 6 tests assessing LCNF optical and mechanical properties (Turbidity, tear resistance, Young's modulus, porosity, and macro size,), and is representative of the global quality of LCNF suspensions.

The equation (Eq. 7) that was adapted for quality index calculation was:

$$Q.I^{*} = 2 \times \text{Turbidity mark} + 2 \times \text{tear resistance mark} + 3 \times \text{Young's modulus mark} + 2 \times \text{porosity mark} + 1 \times \text{micro size mark} \quad (7)$$

where marks are calculated from raw test values as indicated in the work of by Desmaisons et al.[13]. The resulting equation (Eq. 8) including the raw test values was therefore:

$$Q.I^{*} = -0.02 \times X_1 - 7.18 \times \ln(X_2) - 0.108 \times X_3^2 + 3.81 \times X_3 - 0.32 \times X_4 - 5.35 \ln(X_5) + 57.2 \quad (8)$$

with X1 representing the turbidity (NTU), X2 the tear resistance (mN), X3 the Young's modulus (GPa), X4 the porosity (%), and X5 the micro-size (µm²).

3. Results and Discussion

3.1 Effect of enzymatic treatments on fiber properties

Table 2 gives the chemical composition of the Eucalyptus fibers before and after the enzymatic treatments. Xylan was the main non-cellulosic carbohydrate compound found in the samples. Arabinan and Galactan were also found in the hemicellulosic fraction, but in extremely low proportions, while the presence of Mannan was not detected in the analysis.

Table 2. Average and standard deviation of the chemical components content of Eucalyptus fibers before and after enzymatic treatments. *Different letters in the same column indicate significant ($\rho \leq 0.05$) differences between the samples for the Tukey's test. ND = Not detected.

Chemical composition (%)							
Samples	Glu	Hemicellulose				ILig	SLig
		Xyl	Man	Ara	Gal		
UEKP	64 ± 0.1[a]	10 ± 0.01[a]	ND	0.2 ± 0.01[a]	0.5 ± 0.01[a]	17 ± 0.3[a]	3 ± 0.06[a]
LT_UEKP	65 ± 0.2[a]	9 ± 0.07[b]	ND	0.1 ± 0.02[a]	0.4 ± 0.01[a]	17 ± 0.1[a]	3 ± 0.05[a]
LCT_UEKP	63 ± 0.4[b]	10 ± 0.05[a]	ND	0.1 ± 0.00[a]	0.5 ± 0.00[a]	17 ± 0.1[a]	3 ± 0.10[a]

Glu = glucan; Xyl = Xylan; Man = Mannan; Ara = Arabinan; Gal = Galactan; ILig = Insoluble lignin; and SLig = Soluble lignin.

A slight increase (not significant) in the Glucan content was observed in the material treated with the laccase enzyme. This apparent increase is related to the decrease in the content of Xylan in the constitution of the material. The significant reduction in Glucan content after hydrolysis with the endoglucanase enzyme demonstrates that the previous treatment with laccase was effective in modifying the lignin and leaving the cellulose more exposed to the cellulase attack. According to Li et al. [18], the structure of lignin can inhibit the action of enzymes on cellulose through physical barriers, limiting the accessibility of enzymes, inhibiting their hydrolysis. Espinosa et al. [34] produced LCNF from wheat straw with high lignin content (17.7%) with different pretreatments, including enzymatic pretreatment with an endoglucanase

enzyme. The results obtained by these authors show that LCNF pretreated with this enzyme showed the lowest yield of nanofibrillation (37.45%). This corroborates the fact that lignin hinders the action of the enzyme on the cellulose structure, impairing the obtainment of LCNF.

The content of hemicellulose ranged from approximately 11% for UEKP and LCT_UEKP to 9% for LT_UEKP. Dias et al. [25] stated that hemicellulose content in the range of 9 to 12% facilitates cell wall deconstruction. The presence of hemicellulose and its carboxylic groups act to regulate the extent of microfibril aggregation through electrostatic repulsion forces. This acts to facilitate the mechanical nanofibrillation of the fibers.

Regarding the content of insoluble and soluble lignin, no change was observed in its content, showing that the enzymatic load used was able to modify the lignin present in the fiber structure but was not enough to remove it, thus preserving the original content of this macromolecule in the fibers and LCNF obtained.

The MorFi system was used to understand the modifications on fibers' structure before and after the enzymatic hydrolyses. The considered traits were the mean length of fibers, mean fiber width; the proportion of fines based on the length of fines, the fibrillation index, and the fiber coarseness (Table 3).

Table 3. Effect of laccase and cellulase meditated enzymatic hydrolysis treatments of unbleached eucalyptus kraft pulp on fibers' morphological properties. *Different letters in the same column indicate significant ($\rho \leq 0.05$) differences between the samples for the Tukey's test.

Sample	Mean length-weighted length (µm)	Mean fiber width (µm)	Fine's content (%)	Fibrillation index (%)	Mean fiber coarseness (mg/m)
UEKP	620 ± 4^{c}	18.5^{a}	65 ± 1^{a}	3.01 ± 0.01^{c}	0.0938^{a}
LT_UEKP	669 ± 3^{a}	18.3^{b}	55 ± 1^{c}	2.86 ± 0.01^{b}	0.0819^{b}
LCT_UEKP	643 ± 5^{b}	18.6^{a}	62 ± 1^{b}	3.14 ± 0.03^{a}	0.0804^{b}

UEKP = Unbleached eucalyptus kraft pulp without any treatment; LT_UEKP = Laccase treated unbleached eucalyptus kraft pulp and LCT_UEKP = Laccase and cellulase treated unbleached eucalyptus kraft pulp.

Comparing the untreated sample (UEKP) with the one that underwent treatment only with the laccase enzyme (LT_UEKP), there was an increase in the average length of the fibers (from 620 ± 4 to 669 ± 3 µm). Besides, there was a slight decrease in their average width (from 18.5

317 µm to 18.3 µm). Thus, it supports that the laccase enzyme prefers attacking smaller structures
318 present in the suspension, represented by the fines. As shown in Table 1, there was a considerable
319 reduction in the content of fines after laccase-mediated enzymatic hydrolysis.
320 Additionally, according to Chen et al. [35], this behavior, along with the fibrillation
321 indexes, which decreased from 3.01 ± 0.01 to 2.86 ± 0.01% after treatment with laccase, suggests
322 that the enzyme acts more on the surface of the fibers instead of inside. The fact that the enzyme
323 attacked the smaller structures caused the average fiber length to increase.
324 The decrease in coarseness after laccase-mediated enzymatic hydrolysis (from 0.0938 to
325 0.0819 mg/m) can also be observed. The fiber's coarseness measures the amount of fiber per
326 length of fiber, and this parameter indicates the fiber's cell wall thickness, besides how the fiber
327 is being hydrolyzed [36]. From this result, it can be suggested that the first treatment with the
328 laccase enzyme will already facilitate the action of the cellulase enzyme in the subsequent
329 treatment.
330 Analyzing the LCT_UEKP sample, the average length of the fibers increased relative to
331 UEKP, but when compared to the LT_UEKP sample, it decreased in the average length of the
332 same (from 669 ± 3 to 643 ± 5 µm), which indicates that even with the presence of lignin, the
333 cellulase enzyme was able to attack cellulose in the fiber structure. Lignin typically inhibits
334 cellulase enzyme action in cellulose through physical barriers, such as hydrophobicity, surface
335 charges, electrostatic interactions, and interactions between hydrogen bonds [18].
336 Concerning the average fiber width, after the enzymatic treatment using cellulase, the
337 fiber width slightly increased from 18.5 to 18.6 µm, compared to UEKP, and 18.3 to 18.6 µm
338 compared to LT_UEKP. The fines content increased from 55 ± 1% after laccase treatment to 62
339 ± 1% after cellulase treatment. These results indicate that cellulases induce the fibers to swell by
340 attacking the surface and the inner of the fibers, allowing more significant amounts of water
341 molecules into the fibers.
342 The increase in fibrillation index (from 2.86 ± 0.01 to 3.14 ± 0.03%) corroborates the
343 earlier discussion in this section; it indicates that microfibrils are individualized in the fiber cell

wall once again because of the cellulase enzyme action. The value of coarseness for LCT_UEKP also decreased after cellulase hydrolysis (from 0.0819 to 0.0804 mg/m), which agree with the fiber length change, since the longer fibers largely determine the coarseness of a fiber population, and it is more sensitive to changes in the weight of that fraction [36]. According to Azevedo et al. [37], fibers presenting lower coarseness provide a more wettable surface, facilitating water molecules penetration into the fiber structure.

3.2 Visual inspection, stability, and Zeta potential of LCNF suspensions

Sedimentation analysis and the percentage stability over time allowed evaluating the general stability of the aqueous NFC suspensions (Fig. 1).

Fig. 1 here, please

Fig. 1. Dispersion states of the 0.1 wt.% ULCNF and EsT_LCNF suspensions at 0, 10, 30 min, 1, 2, 3, 4, 5, 6, 7, 8, and 24 h. Influence of time on LCNF suspensions stability in water.

Since the existence correlation between particles shapes and sizes, particle agglomerates, and stability, sedimentation analysis has been widely used to evaluate cellulose nanoparticles quality [26]. The sedimentation shows a tendency of enzymes to affect the stability of the suspension during the first 24 hours. As can be seen in Fig. 1, the ULCNF remains highly stable after the first three hours of analysis, showing a stability of 98.6%. On the other hand, the EsT_LCNF starts to suffer a decrease in stability after only 30 minutes and after three hours shows a stability of 84.1%.

After the fourth hour the ULCNF started to show a tendency to decrease the suspension stability and at the end of 8 h, it showed 90% stability while the EsT_LCNF after 8 h showed 78% stability. Interestingly, after 24 h of analysis, both suspensions showed similar stability (77% for ULCNF versus 76% for EsT_LCNF). These results indicate that the ULCNF suspension keeps the dispersed particles in Brownian motion in the suspension longer than the EsT_LCNF. Due to the latter having more repulsion charges as is shown in the Zeta potential values that will be discussed below. Brownian motion tends to randomize the orientation of fibrils when the dispersion is diluted enough, which keeps them dispersed [26].

371 The surface charges of nanofibrils are an important parameter for the use of this material
372 as a reinforcement agent. Nanoparticles must have high Zeta potential, so that the colloidal
373 suspension can resist aggregation, to increase its degree of dispersion in the matrix [38], but,
374 according to Bhattacharjee [39], higher Zeta potential values are not always a guarantee of greater
375 stability in colloidal suspensions, because van der Waals forces that act between particles can
376 promote their agglomeration.

377 The Zeta potential values found for the ULCNF sample was -21.3 ± 0.6 mV and for
378 EsT_LCNF sample was -19.1 ± 0.4 mV, similar to the value that was found by [40] which was -
379 18 ± 3 mV. The Zeta potential of the EsT_LCNF sample was still close to the values found by
380 [41] for NFC obtained after different sodium hydroxide treatments. The values found in this study
381 were higher than those obtained for LCNF found by [42], these authors obtained a Zeta potential
382 of -28.1 ± 1.5 mV.

383 These results indicate that the two suspensions are moderately stable due to the presence
384 of negatively charged carboxyl groups present in the hemicellulose [40]. Zeta-potential
385 measurements give an indication of the stability of the colloidal suspensions. It is assumed that
386 suspensions with a zeta-potential higher than +30mV or lower than -30mV are stable [43].

387 **3.3 Morphological properties of LCNF**

388 The morphology of the obtained LCNF was studied using transmission electron
389 microscopy (Fig. 2). The enzymatic treatments did not cause significant changes in the average
390 diameter of the nanofibrils, but there was a differentiation in the distribution of the diameter
391 ranges of the nanofibrils, as well as in the overall appearance of the nanofibril network of the two
392 samples.

393 **Fig. 2 here, please**

394 **Fig. 2.** Typical transmission electron microscope (TEM) images and diameter distribution of CNF from:
395 A) Untreated Lignin-cellulose nanofibrils (ULCNF), and B) Enzymes treated Lignin-cellulose nanofibrils
396 (EsT_LCNF).

397 Both treatments lead to an efficient fibrillation into micro- and nano-scale
398 elements, the analysis of TEM images enables to determine that these LCNF are

399 composed of bundles of elementary fibrils, with widths between 39 ± 17 nm (ULCNF)
400 and 38 ± 16 nm (EsT_LCNF) and lengths over to 3 μm leading to a high aspect ratio,
401 making this material suitable for polymer reinforcement [44]. Dimensions of these
402 nanofibrils were similar to those reported elsewhere for samples treated by mechanical
403 nanofibrillation [25].

404 Fig. 2 also shows the diameter distribution of LCNF produced in different
405 conditions, with average diameters lower than 30 nm that makes them potentially useful
406 as reinforcing agents in composites [45], the content of LCNF was around 39%, and 45%
407 for ULCNFand EsT_LCNF respectively. These results indicate that the enzyme-treated
408 pulp led to better nanofibrillation and individualization of the fibrils, being the treatment
409 that presented more homogeneous nanofibrils, with 44% of the elements measured within
410 the class of diameter of 15-30 nm. TEM images enable to observe that EsT_LCNF (Fig.
411 4B) shows less nanofibril aggregates compared to ULCNF (Fig. 4A). A lower level of
412 aggregation of LCNF allows them to better interact with polymer matrices via hydrogen
413 bonds. This enhances their mechanical and barrier properties and is attractive in the
414 production of bio nanocomposites [46].

415 **3.4 Rheological behavior**

416 The behavior of the viscosity of the LCNF suspensions was investigated at 25°C. The
417 flow curves and oscillatory tests are shown in Fig. 3.

418 **Fig. 3 here, please**

419 **Fig. 3**. Rheological behavior of LNCF suspensions. A) Apparent viscosity vs. shear rate for the LCNF
420 suspensions, and B) Storage (G') and loss (G'') moduli of suspensions with 1.0% (w/w) LCNF as a function
421 of frequency for: Lignin-cellulose nanofibrils obtained from control) and laccase and cellulase enzymes
422 treated and structural recovery in 3ITT experiments plotted as C) transient viscosity recovery in rotational
423 test, and D) Transient viscosity recovery in rotational test with normalized transient viscosity (η+/η0).

424 The Herschel-Bulkley model was adjusted appropriately for the data of the flow curve (p
425 < 0.001), presenting high values of the coefficient of determination ($R^2 \geq 0.9834$ and $R^2 \geq 0.9932$

for ULCNF and EsT_LCNF respectively). The rheological parameters of the model, as well as the apparent viscosity at 100 s^{-1}, are presented in Table 4.

Table 4. Parameters of the Herschel-Bulkley model and initial apparent viscosity and at 100 s−1 (η100) for ULCNF and EsT_LCNF.

Herschel-Bulkley						
Sample	τ_0 (Pa)	k (Pa.sn)	n (-)	Pr > t	R^2	η100 (mPa.s)
ULCNF	0.90	7.19	0.30	< 0.001	0.9834	303.3 ± 7.6
EsT_LCNF	6.0	2.12	0.36	< 0.001	0.9932	172.3 ± 4.9

ULCNF presented higher value for the consistency index (K) than EsT_LCNF, indicating that this suspension has a higher aspect ratio. The morphology of the material is related to the (K) value, which also explains the lower viscosity of the Est_LCNF (Along with the degree of polymerization), since they present nanofibrils shorter than the ULCNF. Shorter nanofibrils results in a lower stiffness of the network, facilitating its breaking and ordering when subjected to shear, thereby decreasing viscosity [29].

ULCNF presented flow index values of 0.30 while EsT_LCNF presented 0.36. The flow index (n) suggests the entire suspensions' structural property [47], and indicates the degree of non-Newtonian characteristics of the material. According to Du et al. [48] , the increase in the value of (n) in EsT_LCNF is also the result of the decrease in the degree of polymerization of cellulose due to enzymatic action. All the LCNF in the Herschel-Bulkley model point to pseudoplastic fluids' behavior presenting (n) values lower than 1. Similar behavior was reported by Czaikoski et al. [49] when investigating the rheological behavior of cellulose nanofibrils obtained from cassava peel and reported by Souza et al. [29] studying rheological behavior of Pinus, Eucalyptus, and cocoa shell NFC. The decay of viscosity characterizes pseudoplastic fluids as the shear rate applied to the fluid increases (Fig. 3A). It is due to the ordination of the material present in the stable suspension, which is disordered, and, as shear is applied, it starts to become organized, decreasing the system viscosity [30].

Oscillatory shear measurements were performed to identify the response of the viscoelastic properties of the LCNF suspensions. In Fig. 3B, both G′ and G″ were presented as

the functions of frequency at a fixed strain of 0.2% within the linear viscoelastic region. G′ increased with the frequency and it was much larger than G″, which showed a viscoelastic solid-like feature (gel-like properties), indicating that the elastic properties were dominant compared to the viscous properties. Usually, G' is an in-phase elastic modulus associated with energy storage and release in the periodic deformation, and G" is an out of-phase elastic modulus associated with the dissipation of energy [50].

The results show that EsT_LCNF had lower values for G' and G" than ULCNF, which may be related to the action of both enzymes that partially depolymerized both lignin and cellulose, making their rheological properties smaller when compared to the Control. Jordan et al.[51] found similar behavior studying the variations of the degree of polymerization in rheological properties of lignin-containing cellulose nanofibrils from cotton gin motes and cotton gin trash containing high lignin content and after bleaching with $NaOCl_2$ for reduced lignin content. For an ideal gel that behaves elastically, the storage modulus is expected to be independent of frequency and G' > G" [50]. Table 5 shows the storage modulus (G'), gel stiffness (G'/G") and the loss tangent value (tan δ) of LCNF suspensions.

Table 5. Values of storage modulus (G'), gel stiffness (G'/G") and loss tangent value (tan δ(G"/G')) obtained from the mechanical spectra at 25°C and 0.1 rad s-1 for LCNF suspensions at concentrations of 1 wt%.

Samples	Suspension concentration		
	1 wt%		
	G' (Pa)	G'/G''	Tan δ
ULCNF	71.9	6.61	0.15
EsT_LCNF	62.9	7.58	0.13

The EsT_LCNF showed a higher value of G'/G" (7.58) compared to ULCNF (6.61), revealing an increase of the ionic strength of the suspension. According to Naderi and Lindström [52], the stiffening effect might imply a more intimate contact between the nanofibrils, however, the exact mechanism behind this notion is not clear. This behavior may explain the higher value

475 of τ0 for EsT_LCNF when compared to ULCNF. Fig. 4 also shows the dependency of the
476 behavior of G' and G" in relation to the frequency applied for both LCNF investigated.
477 Furthermore, G'/G" values are between 1 and 10, indicating that the materials present gel-
478 like characteristics [29,31]. In this situation, the classic structure is related to the existence of a
479 three-dimensional organization of the molecules that are broken under shear, causing the flow of
480 the material, distinct of true gels, that break under shearing [29].
481 The transition from liquid-like to solid-like behavior for a viscoelastic coating material
482 during immobilization has been described as the maximum slope of the loss factor, which is the
483 ratio of the viscous to elastic modulus [31]. The loss tangent value (tan δ), (G''/G') ratio, was of
484 the order of 0.1 (tan δ <1) for all the samples investigated. This means that the medium is
485 structured in the same way, leading to a gel-like structure. A similar result also was found by
486 Jordan et al. [51].
487 Figs. 3C and 3D show the time-dependent structure regeneration after the removal of a
488 high shear rate. This is an important test because it simulates a practical application of LCNF.
489 The high shear rate in the test reflects the shear rate during a practical application [31].
490 It can be noted that after the breakdown of elastic gel-like structure at high shear during
491 the second interval, both LCNF presented a facility to reorganize and recovery the initial state,
492 even presenting low viscosity than at the beginning of the first interval at a low shear rate. In both
493 cases, the accumulation forces related to the thixotropic behavior of the suspensions and the shear
494 forces compete with each other, causing the interruption of the accumulation structure in progress,
495 resulting in an oscillatory behavior of the recovery curve [53].
496 Lê et al.[53] obtained related results by studying the rheological behavior of suspensions
497 of cellulosic nanofibrils with different lignin levels. They concluded that lignin's presence
498 influences the level of aggregation and elasticity within the nanocellulose gel network, improving
499 the water release properties and increasing the elasticity of the structure. As can be observed in
500 Fig. 4D, EsT_LCNF showed a slightly faster recovery than ULCNF. This result may be due to
501 the laccase enzyme caused the lignin in the fibrils to be made more available on its surfaces or

accessible in the aqueous phase. It facilitated flocculation and aggregation of particles making recovery of the initial characteristics of the suspension faster after the end of the high shear rate, as shows the higher values of (η+/η0) [42]. Moreover, it means that the faster the recuperation of the viscosity, the better is the sagging resistance after application on a rough surface [31]. Understanding the recuperation of the viscosity of LCNF suspensions is essential for the basis of selecting a proper coating procedure.

3.5 Contact angle, wettability, free surface energy and barrier properties

Fig. 4A shows the contact angle (CA) and wettability for the studied LCNF nanopapers.

Fig. 4 here, please

Fig. 4. Average contact angle and wettability values (A) and WVTR and WPA values (B) for untreated and enzymes treated lignin-cellulose nanofibers.

The average contact angles of LCNF nanopapers were 71 ± 4º and 62 ± 5º for ULCNF and EsT_LCNF, respectively. Concerning the wettability properties of the nanopapers, the ULCNF sample reached a value of 0.05 ± 0.01 (°/s) while EsT_LCNF obtained 0.03 ± 0 (°/s). These values were much higher than those found by Nlandu et al. [20], who for LCNF, these authors found a CA of 30, and similar to the result found by Yook et al. [54]. This difference may be due to how the substrates (LCNF) were prepared. In the study by Nlandu and co-workers, these authors prepared films in Petri dishes by the casting method and allowed them to dry overnight at a milder temperature (40°C). Whereas in this study, nanopapers were prepared under vacuum filtration and drying under pressure and elevated temperature, which leads to the formation of a denser and more compact structure with a smaller volume of voids. This causes a more hydrophobic surface, caused by the flow of lignin, which can be more evenly distributed over the surface due to possible plasticization of the lignin under the temperature and humidity conditions used during the nanopaper drying process [43].

On the other hand, the AC results obtained in this study were lower than those found by [1,43], This can be explained by the fact that these authors have used high yield pulps (Thermo Chemi-mechanical) with higher lignin contents than the material used in this study. However, the values obtained in this work are higher than those found in literature for conventional (lignin-

free) nanofibrillated cellulose (NFC). Tayeb et al.[55] found a CA value of 59.4° for NFC, while Solala et al. [56] found ~25° as result for CA, and Wang et al. [57] found a CA of 12º for microfibrillated cellulose (MFC).

Statistically, the use of laccase enzyme as a pre-treatment step did not result in interference with the contact angle and wettability properties of the nanopapers. As it acts depolymerizing the lignin, the enzyme could decrease the hydrophobicity of nanopapers, which was not confirmed. We suspect that the endoglucanase enzyme, by preferentially attacking the amorphous regions of cellulose, leaving the material with more crystalline regions, where fewer sites are available for binding with water molecules, when compared to the amorphous regions of cellulose, may have assisted to compensate for the depolymerization of lignin.

The barrier properties of the lignin-cellulose nanopapers were analyzed in terms of water vapor transmission rate (WVTR) and water vapor permeability (WVP) and the results are shows in Fig. 4B and in the Table 4.

The values for WVTR were 1159 and 1197 g.m². day for ULCNF and EsT_LCNF nanopapers respectively, the samples showed no statistical difference between each other. The EsT_LCNF showed higher WVP property (2.42 g.mm/m². kPa.day) compared to the ULCNF sample that showed a value of 2.07 g.mm/m². kPa.day. These values are in agreement with the values reported by other authors for different raw materials [55,58]. The increase of WVP in EsT_LCNF is since the enzyme laccase, when attacking lignin, ends up decreasing its hydrophobic nature. The presence of lignin reduces the absorption of water molecules during the initial stage of diffusion of water molecules in LCNF nanopapers [58].

On the other hand, some authors in the literature studying the barrier properties (WVTR and WVP) of films from different nanofibrillated cellulose sources with diverse chemical compositions, observed an increase in WVTR for the films containing lignin, which according to the same authors may be due to the lower quality of hydrogen bonds in the films [59]. In addition, the barrier properties of LCNF nanopapers are the result of the combination of their crystalline structure as well as their ability to form dense networks with low porosity [58].

The grease resistance was measured according to the kit test, based on 12 different grease solutions numbered from 1 to 12. The material that achieves oil kit number of 12 is the one that shows the highest grease resistance during the test. According Lavoine et al. [60], a paper is considered grease resistant when it reaches the kit number of 8 or higher. Table 6 report the grease resistance obtained by the LCNF samples.

Table 6. Grease resistance (oil kit number) and surface free energy (SFE) for the nanopapers of ULCNF and EsT_LCNF. *Different letters in the same row indicate significant ($\rho \leq 0.05$) differences between the samples for the Tukey's test.

Characteristic	ULCNF	EsT_LCNF
Oil kit number	12a	12a
SFE (mN/m)	43 ± 3b	47 ± 1a
Disperse (mN/m)	37 ± 5a	37 ± 1a
Polar (mN/m)	6 ± 2b	10 ± 1a

Both samples reached the oil kit number of 12, the same result found by Tayeb et al. [55], indicating that they have the potential to be applied as coating agent in paper and packaging. his result is still indicative of a satisfactory level of nanofibrillation, since the more nanofibrillated the material is, the smaller the pore size in the nanopaper structure makes it more effective at blocking grease and water molecules [57].

Table 6 also show the total surface free energy distinguishing the dispersive and polar contributions. Surface free energy can provide more detailed information about the lignin-cellulose matrix, and it can be calculated from the OWRK model that uses polar and dispersive elements [61]. The surface free energy predicts how well a given solvent wets the surface of a polymer matrix. The increase of the polar component in EsT_LCNF indicates an improvement of their hydrophilic character due to the degradation of non-carbohydrates constituents, more specifically the lignin from the fiber surface. It is known that oxidizing agents react mainly with lignin, breaking unsaturated bonds and producing final carbonyl and carboxyl structures, thus increasing the hydrophilic character of the fibers [62]. In this same context, Steinmetz et al.[21]

demonstrated the potential of laccase as a depolymerizing agent of lignin in a continuous depolymerization process in mild conditions.

Although both samples achieved oil kit number of 12 in the grease resistance test, and the dispersive components of surface free energies remain the same for both samples, behavior that was also observed by Hossain et al.[63], the control sample (ULCNF) seems to be more suitable for application for oil barrier purposes, since it has a lower polar contribution than EsT_LCNF, this means that its surface contains molecules that interact with liquids mainly through dispersive forces, such as Van der Waals interactions [61]. The influence of surface energy in grease resistance was mentioned in recent works by Tayeb et al. and Sheng et al. [55,64]. Fig. 5 show ULCNF presented higher contact angles with polar liquids (water, glycerol, and ethylene-glycol) when compared with EsT_LCNF, leading to lower surface free energy, and a lower surface free energy indicates that fewer solvents can wet the sample surface.

Fig. 5 here, please

Fig. 5. Dynamic nanopaper contact angles for the upper and lower sides of untreated lignin-cellulose nanofibrils (ULCNF) and Enzyme-treated lignin-cellulose nanofibrils (EsT_LCNF). Polar solvents (Deionized water, Glycerol and Ethylene glycol) and apolar solvents (Diiodomethane and 1-bromonaphtalene) were used.

3.6 Energy Consumption

The use of enzymatic pretreatments influenced the energy consumption for producing LCNF suspensions. In comparison to ULCNF, EsT_LCNF promoted a reduction of 42% in energy requirements to produce the nanofibrils, decreasing the consumption of 10.5 kWh/kg to 6.1 kWh.kg. The necessary energy to produce nanocellulose materials is a crucial factor to allow competitive industrial production commercialization of these materials and their derivatives so that they can compete with polymers of petroleum origin. According to Desmaisons et al. [13], since 2008, studies have shown that the use of pretreatments reduces the energy demand for nanofibrillation from 20-30 kWh/kg to 1.0 kWh/kg.

Fig. 6A shows for both samples, energy consumption for mechanical nanofibrillation increases with the extending of grinding passes. The time spent for each pass through the grinder,

608 for all the samples are shown in Fig. 6B. The time for each pass tended to increase during the
609 nanofibrillation process for all treatments.

610 It is interesting to note that the specific nanofibrillation energy for each passage through
611 the grinder of the EsT_LCNF sample is greater than that of the ULCNF. Furthermore, the two
612 energy consumption evolution curves (Fig. 6A) follow a similar trend. In Fig. 6B, the time per
613 passage for the sample treated with the enzymes is also longer compared to the one without
614 treatment. However, even with higher specific energy and nanofibrillation time per pass, the
615 EsT_LCNF sample needed fewer passes (6 against 21 passes) and less time (54 minutes against
616 85 minutes) to reach the gel point than the ULCNF sample, making it consume less overall energy
617 when compared to the control sample.

618 **Fig. 6 here, please**

619 **Fig. 6.** A) Evolution of energy consumption for each pass and B) Time spent vs. nanofibrillation pass for
620 ULCNF and EsT_LCNF. The black arrows indicate the point at which it was observed that the suspensions
621 acquired a consistent gel appearance.

622 One factor that can explain this behavior is that in EsT_LCNF, the fibers' cell wall
623 was delaminated more quickly, making the microfibrils more easily individualized, increasing
624 the water retention capacity of the suspension and, consequently, increasing its viscosity.
625 Furthermore, increasing the nanofibrillation time of the material with each pass through the
626 grinder. This is due to the ability of the cellulose nanoparticles to retain a large amount of water.
627 The increase of viscosity along the nanofibrillation process is a consequence of the disintegration
628 of fibrils, showing a stronger network formation as is typical of cellulose nanoparticles and
629 forming a strong gel structure [65].

630 Literature reports that lignin is one of the most significant factors in the recalcitrance of
631 lignocellulosic biomass [66], a fact that is widely observed during the nanofibrillation of
632 mechanical pulps [65,67]. On the other hand, in the case of chemical pulps, there are reports that
633 the presence of residual lignin can decrease the energy consumption of nanofibrillation [59]. This
634 different behavior between these two types of pulp may be related to the sulfonation of lignin in

635 the compound pulps that allow a more extensive swelling of the fibers by water, accompanied by
636 a more extensive softening of the material [7].

637 **3.7 Quality of lignin-cellulose nanofibrils**

638 The lignin-cellulose nanofibrils produced without and after enzymatic pretreatments were
639 characterized and had their quality evaluated based on the index proposed by Desmaisons et al.
640 [13] obtaining the values shown in Table 7. Despite being originally developed to evaluate
641 suspensions of cellulose nanofibrils from bleached pulps, this index can be applied to LCNF
642 suspensions in order to obtain a broad insight into their qualities, as already reported in the study
643 by Espinosa et al. [58].

644 **Table 7.** Quality indexes of lignin-cellulose nanofibrils produced by different conditions. Different letters
645 in the same column indicate significant ($\rho \leq 0.05$) differences between the samples for the Tukey's test.

Quality index of Lignin-cellulose nanofibrils						
Samples	Turbidity (NTU)	Tear resistance (mN)	Young's modulus (GPa)	Porosity (%)	Micro-size area (µm²)	Q.I*
ULCNF	541 ± 7^{a}	49 ± 3^{a}	7.2 ± 0.3^{b}	29.8 ± 1.7^{a}	73 ± 8^{a}	61 ± 3^{b}
EsT_LCNF	473 ± 5^{b}	41 ± 3^{b}	9.5 ± 0.4^{a}	25.5 ± 1.9^{b}	54 ± 9^{b}	71 ± 2^{a}

646
647 The turbidity is an indirect indicator of the nanofibrillation yield due to the light scattering
648 produced by large particles in a suspension [58]. The enzyme pretreatments promoted a decrease
649 in turbidity in the LCNF suspension (473 ± 5 compared to 541 ± 7 NTU of the untreated sample),
650 a first indication that the material has more nanoscale and less aggregated particles. Similar LCNF
651 turbidity values were found by Amini et al. [4]. When cellulose particles are in nanoscale, they
652 are stable due to Brownian motion, which keeps the particles in suspension caused by the
653 interaction of repelling forces [26].

654 The turbidity measures the light that is dispersed by the material in suspension. As the
655 material becomes smaller, the visible light is not dispersed in the material and the turbidity value
656 tends to approach zero. The opposite happens when the material is composed mostly of particles
657 with larger dimensions in which visible light ends up being dispersed, increasing the turbidity
658 value. According to Foster t al. [68], although turbidity of NFC suspensions is complex due to the

number of scatterers per unit volume, size distribution, and optical properties of the light-scattering bodies, it is consistent method for estimating the quality of nanofibrils.

The mechanical tests results show significance differences on nanopapers properties. The tear resistance result decrease from 49 ± 3 to 41 ± 3 mN after enzymatic hydrolysis, showing the effectiveness of these pretreatments to facilitate the action of the enzyme endoglucanase on the fiber structure that still contains lignin after the action of the enzyme laccase that weakened the lignin structure allowing the effective cutting of fibers and generation of fine elements.

These results present the same tendency as the work of Banvillet et al. [69], where after the use of enzyme hydrolysis, the authors reported decrease of the values of tear resistance. The tear resistance of the nanopapers is related to interactions and dimensions of the LCNF; the more homogeneous the structures are at the nanoscale, more cohesive the material is, facilitating the propagation of the tear by the absence of empty spaces [13].

The Young's modulus was positively affected by the enzymes, the value increased from 7.2 ± 0.3 to 9.5 ± 0.4 GPa where this property is directly influenced by the aspect ratio and interactions of lignin-cellulose nanofibrils. This increase is due to the hydrolysis of the amorphous cellulose in the fibers by the enzymatic action that caused the relative increase of crystalline domains that led to the increase of the stiffness of the material. A similar tendency was observed by Bian et al. [5] where the Young's modulus of LCNF pretreated with endoglucanase and xylanase enzymes increased compared to LCNF produced without any type of treatment (From approximately 3.3 GPa to 4.8 GPa), Ämmälä et al. [70] also produced LCNF with high lignin content from non-delignified Spruce and Pine sawdust after a sulfonation pretreatment, and found stiffness values close to those found in this research (8 GPa for sulfonated Pine LCNF and 7 GPa for sulfonated Spruce).

The enzymatic hydrolysis resulted in a considerable increase of CF, from 59.6 ± 1.7% to 64.6% for EsT_LCNF. This result may indicate that the laccase enzyme was able to partially depolymerize the lignin [21], weakening its structure and avoiding the known inhibitory effect that lignin has on enzymes in cellulosic fibers [18].

686 The increase of crystallinity means that the endoglucanase enzyme was able to attack the
687 amorphous domains of cellulose. It is already reported in several studies that endoglucanase has
688 a preferential action of disordered regions of cellulose than crystalline cellulose [12,71]. This can
689 be confirmed in Table 3 with the decrease in Glucan content in the material treated with the
690 cellulase enzyme. The decrease in Glucan indicates that this polysaccharide molecules were
691 hydrolyzed into Glucose due to the action of the enzyme.
692 Concerning the crystallites size, it was observed that enzymatic hydrolysis led to an
693 increase of crystallites' dimension at the plane (200) from 3.12 ± 0.01 nm to 3.22 ± 0.05 nm. It is
694 expected that after the attack of the amorphous domains of cellulose, enzymes begin to attack the
695 small crystallites [45].The decrease of porosity of the nanopapers (from 29.8% to 25.5%)
696 corroborates with the increase of Young's Modulus after the enzymatic treatments. According to
697 Benítez and Walther [72], this occurs because materials with lower porosity contain more
698 mechanically resistant nanostructures while materials with higher porosity contain air instead of
699 a LCNF network with high mechanical strength. Also according to the same authors and
700 Banvillet et al. [69] with an enzymatic pretreatment, nanopapers with porosities less than 20%
701 and Young's modulus between 8 and 15 GPa are usually obtained.
702 Regarding the micro-size area (µm²), the residual non-nanofibrillated fibers was lower
703 for EsT_LCNF (54 ± 9 µm²), indicating that in this case there was a greater delamination of the
704 cell wall. The pretreatment facilitates the nanofibrillation and leads to the decrease of energy
705 demand. As shown in the previous section, the energy consumption along the nanofibrillation
706 process decreased by 42% after the enzymatic hydrolysis. After determining the quality index for
707 each material, the EsT_LCNF sample achieved a higher value (71 ± 2), with a 10-point advantage
708 over the untreated sample (61 ± 3). Besides the quality of LCNF, an essential factor to produce
709 this material in industrial scale is the energy consumption required for the deconstruction of the
710 lignocellulosic fiber from the macro to the nanoscale. In this study, it was evidenced the
711 effectiveness of the pre-treatments presented as a viable alternative to produce lignocellulosic
712 nanofibrils.

4. Conclusions

This study confirms the positive impact of a combined enzymatic pretreatment of laccase and endoglucanase enzymes for LCNF production. The laccase proved effective in attacking the lignin helping to decrease the recalcitrance of the fiber cell wall and making the cellulose more exposed to physical contact for the action of the endoglucanase. This new pretreatment could therefore be used to produce LCNF in various applications, being attractive for its use in the packaging industry, or for high value-added applications such as substrates for printed electronics. Finally, this pretreatment could be suitable for industrial production, thanks to the decreased energy requirements.

Acknowledgments

The authors thank the Research Support Foundation of Minas Gerais (FAPEMIG), the National Council for Scientific and Technological Development (CNPq), the Brazilian Federal Agency for the Support and Evaluation of Graduate Education (CAPES; Funding Code 001) and the Wood Science and Technology graduate program from Federal University of Lavras for supplying equipment and financial support. We also thank the Laboratoire Génie des Procédés Papetiers (LGP2) is a part of the LabEx Tec 21 (Investissements d'Avenir–grant agreement no. ANR-11-LABX- 0030), Thierry Encinas from CMTC - Grenoble for the XRD analysis and the Center of Microscopy at the Federal University of Minas Gerais (http://www.microscopia.ufmg.br) for providing the equipment and technical support for experiments involving TEM.

Conflict of interest

The authors declare that they have no conflicts of interest.

References

[1] Y. Wen, Z. Yuan, X. Liu, J. Qu, S. Yang, A. Wang, C. Wang, B. Wei, J. Xu, Y. Ni, Preparation and Characterization of Lignin-Containing Cellulose Nanofibril from Poplar High-Yield Pulp via TEMPO-Mediated Oxidation and Homogenization, ACS Sustain. Chem. Eng. 7 (2019) 6131–6139. doi:10.1021/acssuschemeng.8b06355.

[2] Y. Zhao, U. Shakeel, M. Saif Ur Rehman, H. Li, X. Xu, J. Xu, Lignin-carbohydrate

742 complexes (LCCs) and its role in biorefinery, J. Clean. Prod. 253 (2020) 120076.
743 doi:10.1016/j.jclepro.2020.120076.

744 [3] A. Lorenci Woiciechowski, C.J. Dalmas Neto, L. Porto de Souza Vandenberghe,
745 D.P. de Carvalho Neto, A.C. Novak Sydney, L.A.J. Letti, S.G. Karp, L.A. Zevallos
746 Torres, C.R. Soccol, Lignocellulosic biomass: Acid and alkaline pretreatments and
747 their effects on biomass recalcitrance – Conventional processing and recent
748 advances, Bioresour. Technol. 304 (2020) 122848.
749 doi:10.1016/j.biortech.2020.122848.

750 [4] E. Amini, I. Hafez, M. Tajvidi, D.W. Bousfield, Cellulose and lignocellulose
751 nanofibril suspensions and films: A comparison, Carbohydr. Polym. 250 (2020)
752 117011. doi:10.1016/j.carbpol.2020.117011.

753 [5] H. Bian, L. Chen, M. Dong, Y. Fu, R. Wang, X. Zhou, X. Wang, J. Xu, H. Dai,
754 Cleaner production of lignocellulosic nanofibrils: Potential of mixed enzymatic
755 treatment, J. Clean. Prod. 270 (2020) 122506. doi:10.1016/j.jclepro.2020.122506.

756 [6] A. Gupta, W. Simmons, G.T. Schueneman, D. Hylton, E.A. Mintz, Rheological
757 and thermo-mechanical properties of poly(lactic acid)/lignin-coated cellulose
758 nanocrystal composites, ACS Sustain. Chem. Eng. 5 (2017) 1711–1720.
759 doi:10.1021/acssuschemeng.6b02458.

760 [7] I. Solala, M.C. Iglesias, M.S. Peresin, On the potential of lignin-containing
761 cellulose nanofibrils (LCNFs): a review on properties and applications, Cellulose.
762 8 (2019). doi:10.1007/s10570-019-02899-8.

763 [8] H. Bian, L. Chen, M. Dong, L. Wang, R. Wang, X. Zhou, C. Wu, X. Wang, X. Ji,
764 H. Dai, Natural lignocellulosic nanofibril film with excellent ultraviolet blocking
765 performance and robust environment resistance, Int. J. Biol. Macromol. 166 (2021)
766 1578–1585. doi:10.1016/j.ijbiomac.2020.11.037.

767 [9] A.K. Kumar, S. Sharma, Recent updates on different methods of pretreatment of
768 lignocellulosic feedstocks: a review, Bioresour. Bioprocess. 4 (2017).
769 doi:10.1186/s40643-017-0137-9.

770 [10] M. Henriksson, G. Henriksson, L.A. Berglund, T. Lindström, An environmentally
771 friendly method for enzyme-assisted preparation of microfibrillated cellulose
772 (MFC) nanofibers, Eur. Polym. J. 43 (2007) 3434–3441.
773 doi:10.1016/j.eurpolymj.2007.05.038.

774 [11] M. Pääkko, M. Ankerfors, H. Kosonen, A. Nykänen, S. Ahola, M. Österberg, J.
775 Ruokolainen, J. Laine, P.T. Larsson, O. Ikkala, T. Lindström, Enzymatic
776 hydrolysis combined with mechanical shearing and high-pressure homogenization
777 for nanoscale cellulose fibrils and strong gels, Biomacromolecules. 8 (2007) 1934–
778 1941. doi:10.1021/bm061215p.

779 [12] O. Nechyporchuk, F. Pignon, M.N. Belgacem, Morphological properties of
780 nanofibrillated cellulose produced using wet grinding as an ultimate fibrillation
781 process, J. Mater. Sci. 50 (2015) 531–541. doi:10.1007/s10853-014-8609-1.

782 [13] J. Desmaisons, E. Boutonnet, M. Rueff, A. Dufresne, J. Bras, A new quality index

783 for benchmarking of different cellulose nanofibrils, Carbohydr. Polym. 174 (2017)
784 318–329. doi:10.1016/j.carbpol.2017.06.032.

785 [14] G.L. Berto, B.D. Mattos, O.J. Rojas, V. Arantes, Single-Step Fiber Pretreatment
786 with Monocomponent Endoglucanase: Defibrillation Energy and Cellulose
787 Nanofibril Quality, ACS Sustain. Chem. Eng. (2021).
788 doi:10.1021/acssuschemeng.0c08162.

789 [15] M. Hassan, L. Berglund, E. Hassan, R. Abou-Zeid, K. Oksman, Effect of xylanase
790 pretreatment of rice straw unbleached soda and neutral sulfite pulps on isolation of
791 nanofibers and their properties, Cellulose. 25 (2018) 2939–2953.
792 doi:10.1007/s10570-018-1779-2.

793 [16] S. Koskela, S. Wang, D. Xu, X. Yang, K. Li, L.A. Berglund, L.S. McKee, V.
794 Bulone, Q. Zhou, Lytic polysaccharide monooxygenase (LPMO) mediated
795 production of ultra-fine cellulose nanofibres from delignified softwood fibres,
796 Green Chem. 21 (2019) 5924–5933. doi:10.1039/c9gc02808k.

797 [17] M.H. Sipponen, J. Rahikainen, T. Leskinen, V. Pihlajaniemi, M.-L. Mattinen, H.
798 Lange, C. Crestini, M. Österberg, Structural changes of lignin in biorefinery
799 pretreatments and consequences to enzyme-lignin interactions, Nord. Pulp Pap.
800 Res. J. 32 (2017) 550–571. doi:10.3183/npprj-2017-32-04-p550-571.

801 [18] M. Li, L. Yi, L. Bin, Q. Zhang, J. Song, H. Jiang, C. Chen, S. Wang, D. Min,
802 Comparison of nonproductive adsorption of cellulase onto lignin isolated from
803 pretreated lignocellulose, Cellulose. 27 (2020) 7911–7927. doi:10.1007/s10570-
804 020-03357-6.

805 [19] A.C. Rodrigues, A.F. Leitão, S. Moreira, C. Felby, M. Gama, Recycling of
806 cellulases in lignocellulosic hydrolysates using alkaline elution, Bioresour.
807 Technol. 110 (2012) 526–533. doi:10.1016/j.biortech.2012.01.140.

808 [20] H. Nlandu, K. Belkacemi, N. Chorfa, S. Elkoun, M. Robert, S. Hamoudi, Laccase-
809 Mediated Grafting of Phenolic Compounds onto Lignocellulosic Flax Nanofibers,
810 J. Nat. Fibers. 00 (2020) 1–10. doi:10.1080/15440478.2020.1738307.

811 [21] V. Steinmetz, M. Villain-gambier, A. Klem, I. Ziegler, S. Dumarcay, D. Trebouet,
812 In-situ extraction of depolymerization products by membrane filtration against
813 lignin condensation, Bioresour. Technol. 311 (2020) 123530.
814 doi:10.1016/j.biortech.2020.123530.

815 [22] G. Singh, S.K. Arya, Utility of laccase in pulp and paper industry: A progressive
816 step towards the green technology, Int. J. Biol. Macromol. 134 (2019) 1070–1084.
817 doi:10.1016/j.ijbiomac.2019.05.168.

818 [23] R.P. Chandra, L.K. Lehtonen, A.J. Ragauskas, Modification of High Lignin
819 Content Kraft Pulps with Laccase to Improve Paper Strength Properties. 1. Laccase
820 Treatment in the Presence of Gallic Acid, Biotechnol. Prog. 20 (2004) 255–261.
821 doi:10.1021/bp0300366.

822 [24] J. Jiang, W. Ye, L. Liu, Z. Wang, Y. Fan, T. Saito, A. Isogai, Cellulose Nanofibers
823 Prepared Using the TEMPO/Laccase/O2 System, Biomacromolecules. 18 (2017)

824 288–294. doi:10.1021/acs.biomac.6b01682.

825 [25] M.C. Dias, M.C. Mendonça, R.A.P. Damásio, Influence of hemicellulose content
826 of Eucalyptus and Pinus fibers on the grinding process for obtaining cellulose
827 micro / nanofibrils, Holzforschung. 73 (2019) 1035–1046.

828 [26] L.E. Silva, A. de A. dos Santos, L. Torres, Z. McCaffrey, A. Klamczynski, G.
829 Glenn, A.R. de Sena Neto, D. Wood, T. Williams, W. Orts, R.A.P. Damásio,
830 G.H.D. Tonoli, Redispersion and structural change evaluation of dried
831 microfibrillated cellulose, Carbohydr. Polym. 252 (2021).
832 doi:10.1016/j.carbpol.2020.117165.

833 [27] Y. Nishiyama, P. Langan, H. Chanzy, Crystal Structure and Hydrogen-Bonding
834 System in Cellulose Iβ from Synchrotron X-ray and Neutron Fiber Diffraction, J.
835 Am. Chem. Soc. 124 (2002) 9074–9082. doi:10.1021/ja0257319.

836 [28] A.D. French, Increment in evolution of cellulose crystallinity analysis, Cellulose.
837 27 (2020) 5445–5448. doi:10.1007/s10570-020-03172-z.

838 [29] L.O. Souza, O.A. Lessa, M.C. Dias, G.H.D. Tonoli, D.V.B. Rezende, M.A.
839 Martins, I.C.O. Neves, J.V. de Resende, E.E.N. Carvalho, E.V. de Barros Vilas
840 Boas, J.R. de Oliveira, M. Franco, Study of morphological properties and
841 rheological parameters of cellulose nanofibrils of cocoa shell (Theobroma cacao
842 L.), Carbohydr. Polym. 214 (2019). doi:10.1016/j.carbpol.2019.03.037.

843 [30] J.F. Steffe, Rheological methods in food process engineering, Freeman Press,
844 Michigan, 1996.

845 [31] K. Dimic-Misic, P.A.C. Gane, J. Paltakari, Micro and nanofibrillated cellulose as
846 a rheology modifier additive in CMC-containing pigment-coating formulations,
847 Ind. Eng. Chem. Res. 52 (2013) 16066–16083. doi:10.1021/ie4028878.

848 [32] J. Rantanen, K. Dimic-Misic, J. Pirttiniemi, P. Kuosmanen, T.C. Maloney,
849 Forming and dewatering of a microfibrillated cellulose composite paper,
850 BioResources. 10 (2015) 3492–3506. doi:10.15376/biores.10.2.3492-3506.

851 [33] D.K. Owens, R.C. Wendt, Estimation of the surface free energy of polymers, J.
852 Appl. Polym. Sci. 13 (1969) 1741–1747. doi:10.1002/app.1969.070130815.

853 [34] A. Espinosa, E., Domínguez, J., Sánchez, R., Tarrés, Q., Rodríguez, The effect of
854 pre-treatment on the production of lignocellulosic nanofibers and their application
855 as a reinforcing agent in paper, (2017) 2605–2618. doi:10.1007/s10570-017-1281-
856 2.

857 [35] G. Chen, J. Dong, J. Wan, Y. Ma, Y. Wang, Fiber characterization of old
858 corrugated container bleached pulp with laccase and glycine pretreatment,
859 Biomass Convers. Biorefinery. (2021). doi:10.1007/s13399-020-01200-3.

860 [36] C.A. Mooney, S.D. Mansfield, R.P. Beatson, J.N. Saddler, The effect of fiber
861 characteristics on hydrolysis and cellulase accessibility to softwood substrates,
862 Enzyme Microb. Technol. 25 (1999) 644–650. doi:10.1016/S0141-
863 0229(99)00098-8.

[37] C.A. Azevedo, S.M.C. Rebola, E.M. Domingues, F.M.L. Figueiredo, D. V. Evtuguin, Relationship between Surface Properties and Fiber Network Parameters of Eucalyptus Kraft Pulps and Their Absorption Capacity, Surfaces. 3 (2020) 265–281. doi:10.3390/surfaces3030020.

[38] H. Tibolla, F.M. Pelissari, F.C. Menegalli, Cellulose nanofibers produced from banana peel by chemical and enzymatic treatment, LWT - Food Sci. Technol. 59 (2014) 1311–1318. doi:10.1016/j.lwt.2014.04.011.

[39] S. Bhattacharjee, Review article DLS and zeta potential – What they are and what they are not ?, J. Control. Release. 235 (2016) 337–351. doi:10.1016/j.jconrel.2016.06.017.

[40] R. Bardet, C. Reverdy, N. Belgacem, I. Leirset, K. Syverud, M. Bardet, J. Bras, Substitution of nanoclay in high gas barrier films of cellulose nanofibrils with cellulose nanocrystals and thermal treatment, Cellulose. 22 (2015) 1227–1241. doi:10.1007/s10570-015-0547-9.

[41] H. Lee, J. Sundaram, L. Zhu, Y. Zhao, S. Mani, Improved thermal stability of cellulose nano fi brils using low-concentration alkaline pretreatment, Carbohydr. Polym. 181 (2018) 506–513. doi:10.1016/j.carbpol.2017.08.119.

[42] M. Imani, K. Dimic-Misic, M. Tavakoli, O.J. Rojas, P.A.C. Gane, Coupled Effects of Fibril Width, Residual and Mechanically Liberated Lignin on the Flow, Viscoelasticity, and Dewatering of Cellulosic Nanomaterials, Biomacromolecules. 21 (2020) 4123–4134. doi:10.1021/acs.biomac.0c00918.

[43] M. Herrera, K. Thitiwutthisakul, X. Yang, P. on Rujitanaroj, R. Rojas, L. Berglund, Preparation and evaluation of high-lignin content cellulose nanofibrils from eucalyptus pulp, Cellulose. 25 (2018) 3121–3133. doi:10.1007/s10570-018-1764-9.

[44] Y.M. Zhou, S.Y. Fu, L.M. Zheng, H.Y. Zhan, Effect of nanocellulose isolation techniques on the formation of reinforced poly(vinyl alcohol) nanocomposite films, Express Polym. Lett. 6 (2012) 794–804. doi:10.3144/expresspolymlett.2012.85.

[45] G.H.D. Tonoli, K.M. Holtman, G. Glenn, A.S. Fonseca, D. Wood, T. Williams, V.A. Sa, L. Torres, A. Klamczynski, W.J. Orts, Properties of cellulose micro/nanofibers obtained from eucalyptus pulp fiber treated with anaerobic digestate and high shear mixing, Cellulose. 23 (2016) 1239–1256. doi:10.1007/s10570-016-0890-5.

[46] R.C. do Lago, A.L.M. de Oliveira, M. Cordasso Dias, E.E.N. de Carvalho, G.H. Denzin Tonoli, E.V. de Barros Vilas Boas, Obtaining cellulosic nanofibrils from oat straw for biocomposite reinforcement: Mechanical and barrier properties, Ind. Crops Prod. 148 (2020). doi:10.1016/j.indcrop.2020.112264.

[47] A.I. Koponen, The effect of consistency on the shear rheology of aqueous suspensions of cellulose micro- and nanofibrils: a review, Cellulose. 27 (2020) 1879–1897. doi:10.1007/s10570-019-02908-w.

[48] J. Du, F. Zhang, Y. Li, H. Zhang, J. Liang, H. Zheng, H. Huang, Enzymatic liquefaction and saccharification of pretreated corn stover at high-solids concentrations in a horizontal rotating bioreactor, Bioprocess Biosyst. Eng. 37 (2014) 173–181. doi:10.1007/s00449-013-0983-6.

[49] A. Czaikoski, R.L. da Cunha, F.C. Menegalli, Rheological behavior of cellulose nanofibers from cassava peel obtained by combination of chemical and physical processes, Carbohydr. Polym. 248 (2020) 116744. doi:10.1016/j.carbpol.2020.116744.

[50] C. Qiao, G. Chen, J. Zhang, J. Yao, Structure and rheological properties of cellulose nanocrystals suspension, Food Hydrocoll. 55 (2016) 19–25. doi:10.1016/j.foodhyd.2015.11.005.

[51] J.H. Jordan, M.W. Easson, S. Thompson, Q. Wu, B.D. Condon, Lignin-containing cellulose nanofibers with gradient lignin content obtained from cotton gin motes and cotton gin trash, Cellulose. 28 (2021) 757–773. doi:10.1007/s10570-020-03549-0.

[52] A. Naderi, T. Lindström, A comparative study of the rheological properties of three different nanofibrillated cellulose systems, 31 (2016).

[53] H.Q. Lê, K. Dimic-Misic, L.S. Johansson, T. Maloney, H. Sixta, Effect of lignin on the morphology and rheological properties of nanofibrillated cellulose produced from γ-valerolactone/water fractionation process, Cellulose. 25 (2018) 179–194. doi:10.1007/s10570-017-1602-5.

[54] S. Yook, H. Park, H. Park, S.Y. Lee, J. Kwon, H.J. Youn, Barrier coatings with various types of cellulose nanofibrils and their barrier properties, Cellulose. 27 (2020) 4509–4523. doi:10.1007/s10570-020-03061-5.

[55] A.H. Tayeb, M. Tajvidi, D. Bousfield, Paper-based oil barrier packaging using lignin-containing cellulose nanofibrils, Molecules. 25 (2020). doi:10.3390/molecules25061344.

[56] I. Solala, R. Bordes, A. Larsson, Water vapor mass transport across nanofibrillated cellulose films: effect of surface hydrophobization, Cellulose. 25 (2018) 347–356. doi:10.1007/s10570-017-1608-z.

[57] W. Wang, F. Gu, Z. Deng, Y. Zhu, J. Zhu, T. Guo, J. Song, H. Xiao, Multilayer surface construction for enhancing barrier properties of cellulose-based packaging, Carbohydr. Polym. 255 (2021) 117431. doi:10.1016/j.carbpol.2020.117431.

[58] E. Espinosa, F. Rol, J. Bras, A. Rodríguez, Use of multi-factorial analysis to determine the quality of cellulose nanofibers: effect of nanofibrillation treatment and residual lignin content, Cellulose. 3 (2020). doi:10.1007/s10570-020-03136-3.

[59] K.L. Spence, R.A. Venditti, O.J. Rojas, Y. Habibi, J.J. Pawlak, A comparative study of energy consumption and physical properties of microfibrillated cellulose produced by different processing methods, Cellulose. 18 (2011) 1097–1111. doi:10.1007/s10570-011-9533-z.

946 [60] N. Lavoine, I. Desloges, B. Khelifi, J. Bras, Impact of different coating processes
947 of microfibrillated cellulose on the mechanical and barrier properties of paper, J.
948 Mater. Sci. 49 (2014) 2879–2893. doi:10.1007/s10853-013-7995-0.

949 [61] S.P.L. Balasubramaniam, A.S. Patel, B. Nayak, Surface modification of cellulose
950 nanofiber film with fatty acids for developing renewable hydrophobic food
951 packaging, Food Packag. Shelf Life. 26 (2020) 100587.
952 doi:10.1016/j.fpsl.2020.100587.

953 [62] G.H.D. Tonoli, M.N. Belgacem, J. Bras, M.A. Pereira-Da-Silva, F.A. Rocco Lahr,
954 H. Savastano, Impact of bleaching pine fibre on the fibre/cement interface, J.
955 Mater. Sci. 47 (2012) 4167–4177. doi:10.1007/s10853-012-6271-z.

956 [63] R. Hossain, M. Tajvidi, D. Bousfield, D.J. Gardner, Multi-layer oil-resistant food
957 serving containers made using cellulose nanofiber coated wood flour composites,
958 Carbohydr. Polym. 267 (2021) 118221. doi:10.1016/j.carbpol.2021.118221.

959 [64] J. Sheng, J. Li, L. Zhao, Fabrication of grease resistant paper with non-fluorinated
960 chemicals for food packaging, Cellulose. 26 (2019) 6291–6302.
961 doi:10.1007/s10570-019-02504-y.

962 [65] P. Lahtinen, S. Liukkonen, J. Pere, A. Sneck, H. Kangas, A Comparative study of
963 fibrillated fibers from different mechanical and chemical pulps, BioResources. 9
964 (2014) 2115–2127. doi:10.15376/biores.9.2.2115-2127.

965 [66] M. Li, Y. Pu, A.J. Ragauskas, Current Understanding of the Correlation of Lignin
966 Structure with Biomass Recalcitrance, Front. Chem. 4 (2016) 1–8.
967 doi:10.3389/fchem.2016.00045.

968 [67] M. He, G. Yang, J. Chen, X. Ji, Q. Wang, Production and Characterization of
969 Cellulose Nanofibrils from Different Chemical and Mechanical Pulps, J. Wood
970 Chem. Technol. 38 (2018) 149–158. doi:10.1080/02773813.2017.1411368.

971 [68] E.J. Foster, R.J. Moon, U.P. Agarwal, M.J. Bortner, J. Bras, S. Camarero-Espinosa,
972 K.J. Chan, M.J.D. Clift, E.D. Cranston, S.J. Eichhorn, D.M. Fox, W.Y. Hamad, L.
973 Heux, B. Jean, M. Korey, W. Nieh, K.J. Ong, M.S. Reid, S. Renneckar, R. Roberts,
974 J.A. Shatkin, J. Simonsen, K. Stinson-Bagby, N. Wanasekara, J. Youngblood,
975 Current characterization methods for cellulose nanomaterials, Chem. Soc. Rev. 47
976 (2018) 2609–2679. doi:10.1039/c6cs00895j.

977 [69] G. Banvillet, E. Gatt, N. Belgacem, J. Bras, Cellulose fibers deconstruction by
978 twin-screw extrusion with in situ enzymatic hydrolysis via bioextrusion,
979 Bioresour. Technol. 327 (2021) 124819. doi:10.1016/j.biortech.2021.124819.

980 [70] Ä. Ari, J.A. Sirviö, H. Liimatainen, Energy consumption, physical properties and
981 reinforcing ability of microfibrillated cellulose with high lignin content made from
982 non-delignified spruce and pine sawdust, Ind. Crop. Prod. 170 (2021).

983 [71] K.R. Hakeem, M. Jawaid, O.Y. Alothman, Rheological Properties and Processing
984 of Polymer Blends with Micro- and Nanofibrillated Cellulose, 2015.
985 doi:10.1007/978-3-319-13847-3.

986 [72] A.J. Benítez, A. Walther, Cellulose nanofibril nanopapers and bioinspired

nanocomposites: A review to understand the mechanical property space, J. Mater. Chem. A. 5 (2017) 16003–16024. doi:10.1039/c7ta02006f.

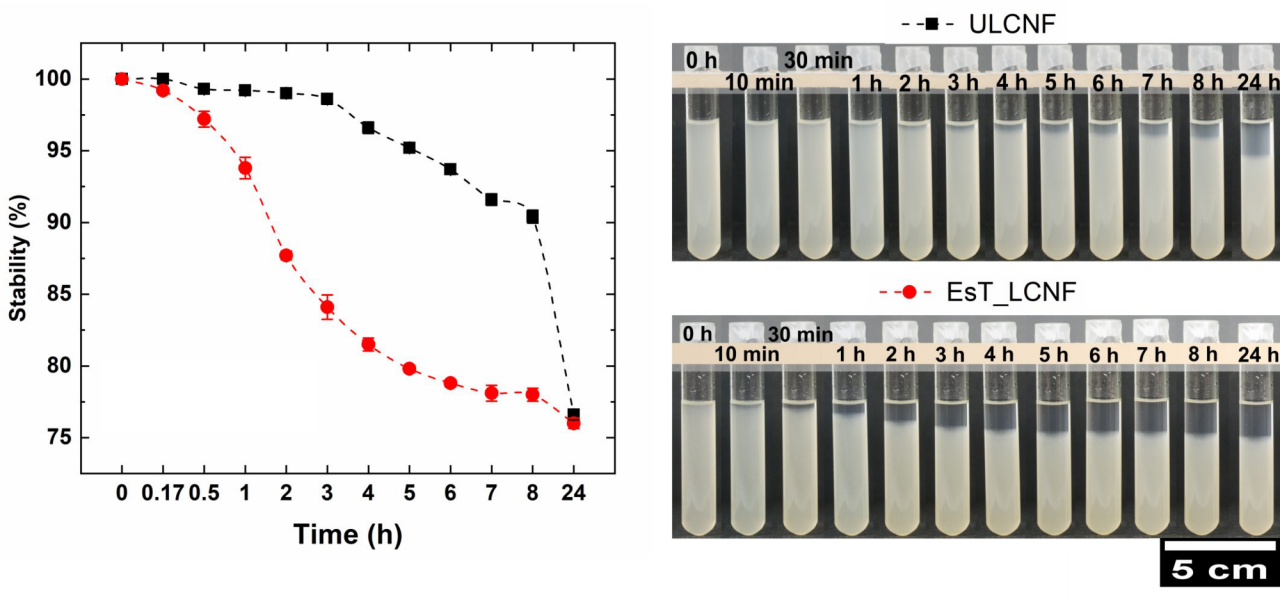
Stability (%)
100
95
90
85
80
75
0
0.17
0.5
1
2
3
4
5
6
7
8
24
Time (h)
ULCNF
0 h
30 min
10 min
1 h
2 h
3 h
4 h
5 h
6 h
7 h
8 h
24 h
EsT_LCNF
0 h
30 min
10 min
1 h
2 h
3 h
4 h
5 h
6 h
7 h
8 h
24 h
5 cm

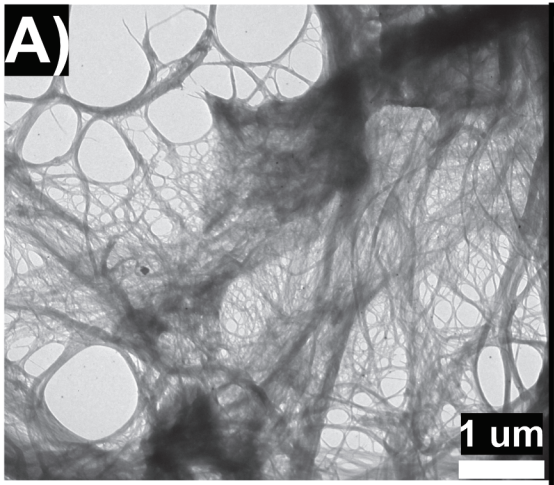
A)
1 um

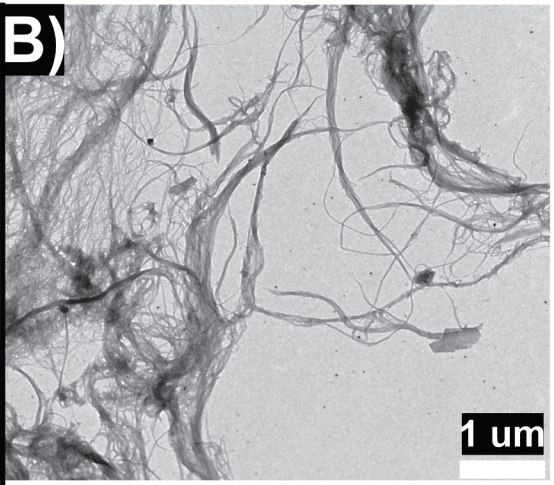
B)
1 um

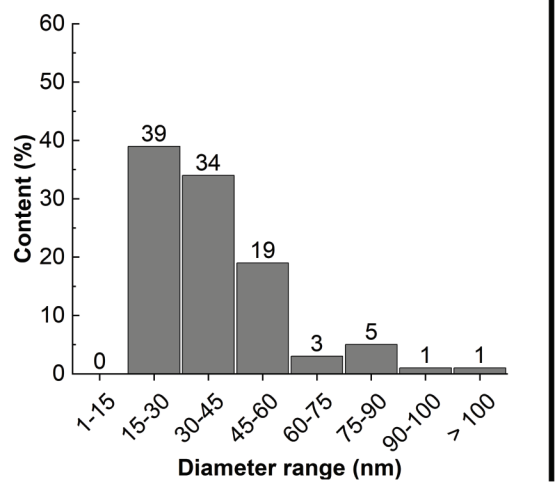
Content (%)
60
50
40
30
20
10
0
39
34
19
3
5
1
1
0
1-15
15-30
30-45
45-60
60-75
75-90
90-100
> 100
Diameter range (nm)

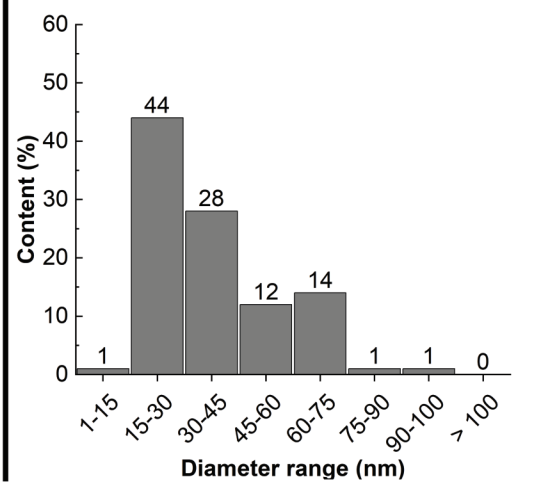
Content (%)
60
50
40
30
20
10
0
44
28
12
14
1
1
1
0
1-15
15-30
30-45
45-60
60-75
75-90
90-100
> 100
Diameter range (nm)

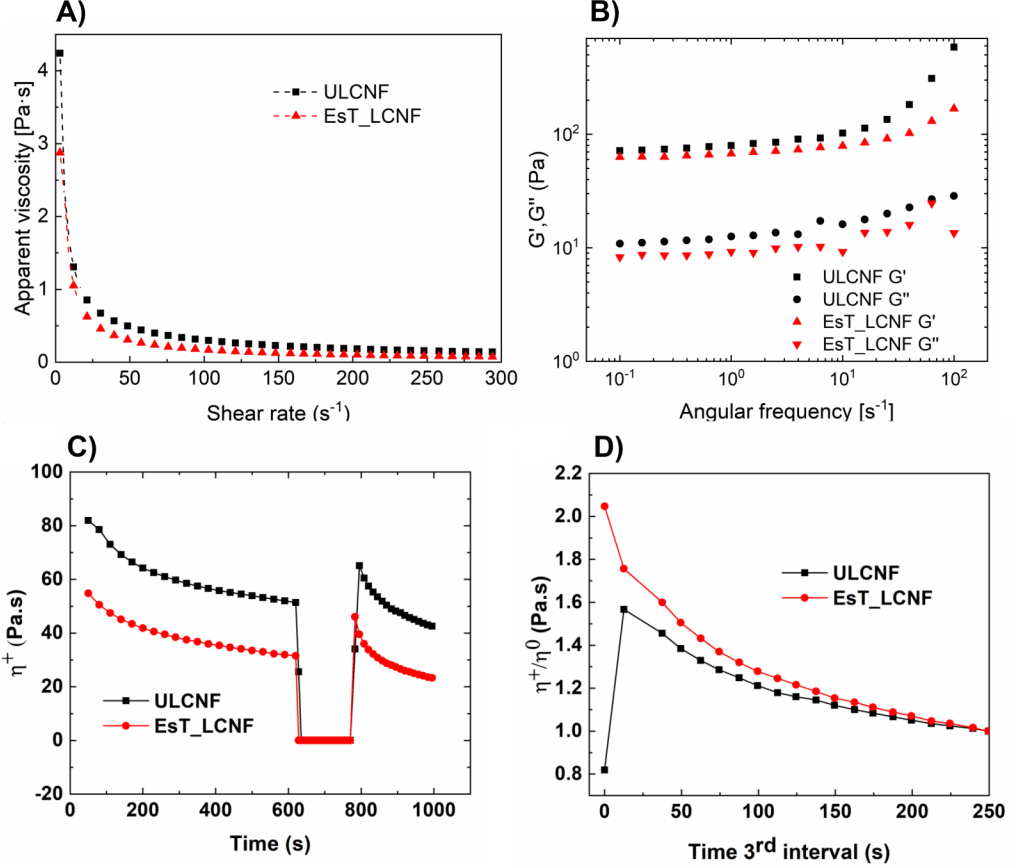
A)
Apparent viscosity [Pa·s]
Shear rate (s-1)
ULCNF
EsT_LCNF
B)
G',G'' (Pa)
Angular frequency [s-1]
ULCNF G'
ULCNF G''
EsT_LCNF G'
EsT_LCNF G''
C)
η+ (Pa.s)
Time (s)
ULCNF
EsT_LCNF
D)
η+/η0 (Pa.s)
Time 3rd interval (s)
ULCNF
EsT_LCNF

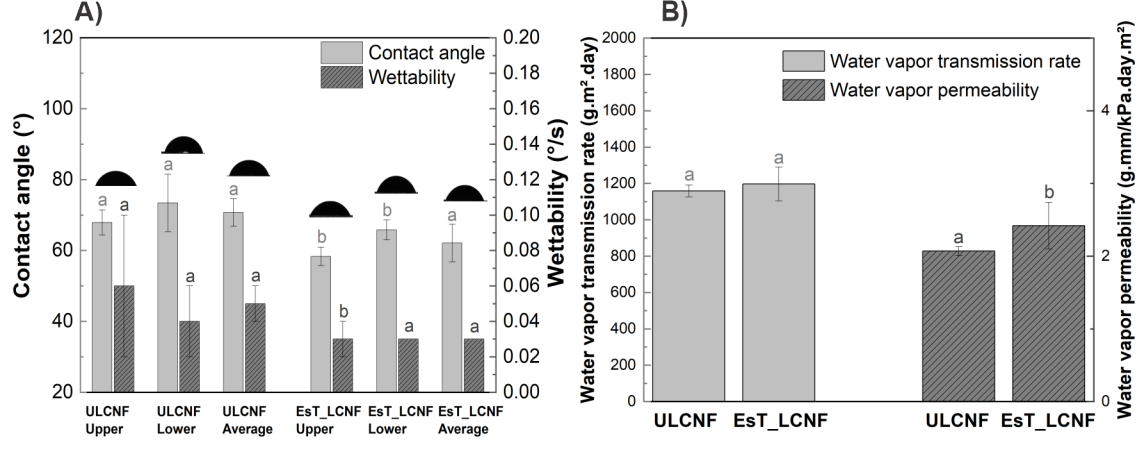
A)
Contact angle
Wettability
Contact angle (°)
Wettability (°/s)
120
100
80
60
40
20
0.20
0.18
0.16
0.14
0.12
0.10
0.08
0.06
0.04
0.02
0.00
a
a
a
a
a
b
b
a
b
a
a
a
ULCNF Upper
ULCNF Lower
ULCNF Average
EsT_LCNF Upper
EsT_LCNF Lower
EsT_LCNF Average
B)
Water vapor transmission rate
Water vapor permeability
Water vapor transmission rate (g.m².day)
Water vapor permeability (g.mm/kPa.day.m²)
2000
1800
1600
1400
1200
1000
800
600
400
200
0
4
2
0
a
a
a
b
ULCNF
EsT_LCNF
ULCNF
EsT_LCNF

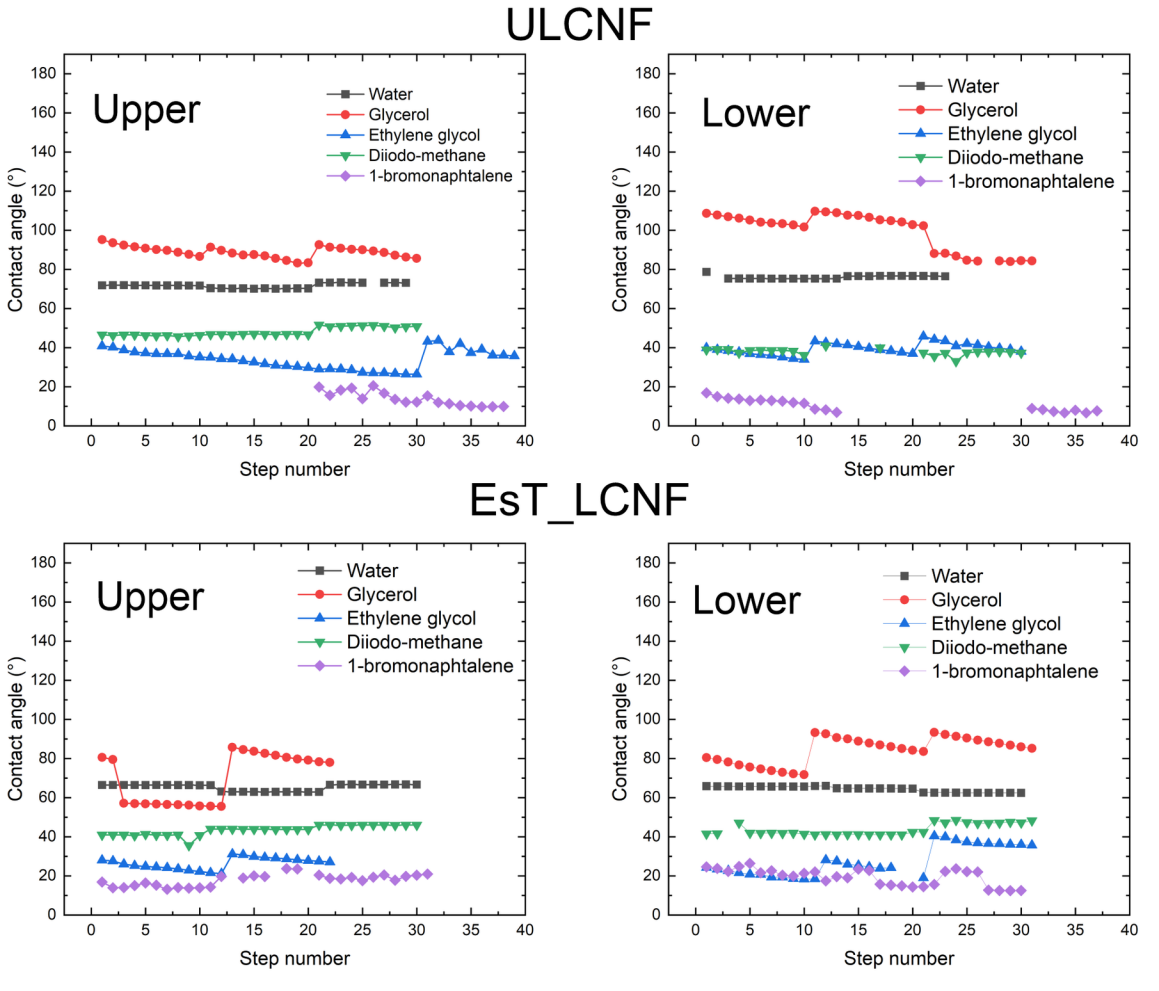
ULCNF
Upper
Lower
EsT_LCNF
Upper
Lower
Water
Glycerol
Ethylene glycol
Diiodo-methane
1-bromonaphtalene
Contact angle (°)
Step number

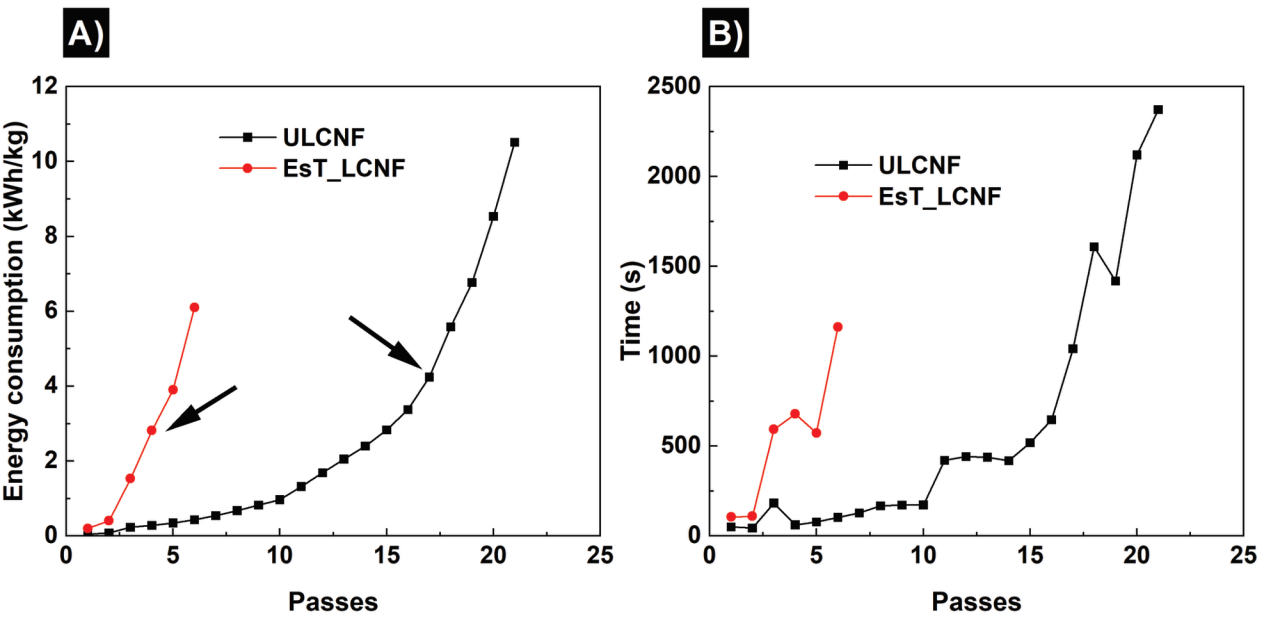
A)
B)
ULCNF
EsT_LCNF
Energy consumption (kWh/kg)
Time (s)
Passes
Passes
0
2
4
6
8
10
12
0
500
1000
1500
2000
2500
0
5
10
15
20
25

Pulping

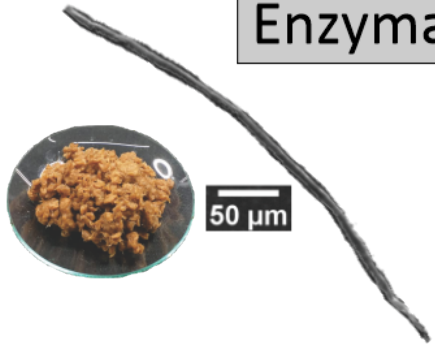

Enzymatic pretreatments

Nanofibrillation

ULCNF

EsT_LCNF

Drying

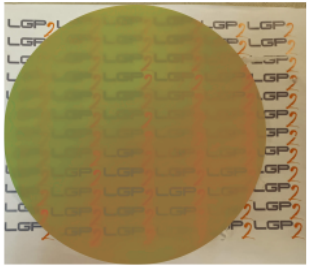

Nanopaper